Report

Current Biology

Loss and Re-emergence of Legs in Snakes by Modular Evolution of *Sonic hedgehog* and *HOXD* Enhancers

Graphical Abstract

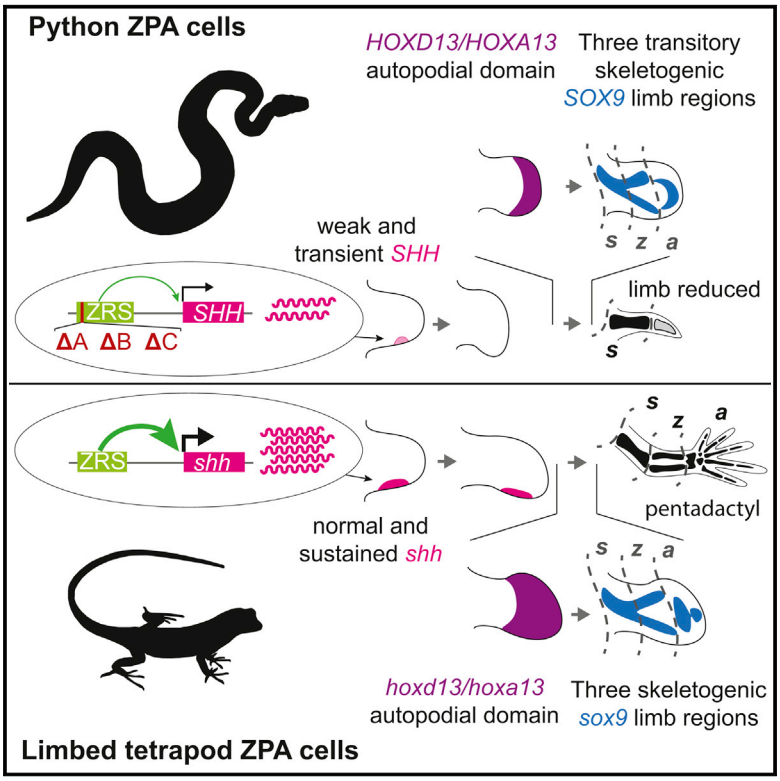

Highlights

- Python legs are truncated due to early arrest of *Sonic hedgehog (SHH)* transcription
- The python *SHH* limb enhancer has weak activity due to deletion of key binding sites
- *HOXD* digit enhancers and the footplate expression domain are conserved in pythons
- Python leg buds form transitory condensations of the tibia, fibula, and footplate

Authors

Francisca Leal, Martin J. Cohn

Correspondence

mjcohn@ufl.edu

In Brief

Leal and Cohn show that hindlimb development arrests in pythons due to mutations in an enhancer that controls *Sonic hedgehog* transcription in limb buds. In contrast, *HOXD* limb enhancers and distal expression are conserved, and pythons form a transitory foot skeleton, providing insights into how legs were lost and then regained in snake evolution.

Accession Numbers

KX778812
KX778839
KX824111
KX824112

Leal & Cohn, 2016, Current Biology *26*, 2966–2973
November 7, 2016
http://dx.doi.org/10.1016/j.cub.2016.09.020

CellPress

Current Biology
Report

Loss and Re-emergence of Legs in Snakes by Modular Evolution of *Sonic hedgehog* and *HOXD* Enhancers

Francisca Leal[1,2] and Martin J. Cohn[1,2,3,4,*]
[1]Howard Hughes Medical Institute
[2]Department of Biology
[3]Department of Molecular Genetics and Microbiology
UF Genetics Institute, University of Florida, P.O. Box 103610, University of Florida, Gainesville, FL 32610, USA
[4]Lead Contact
*Correspondence: mjcohn@ufl.edu
http://dx.doi.org/10.1016/j.cub.2016.09.020

SUMMARY

Limb reduction and loss are hallmarks of snake evolution. Although advanced snakes are completely limbless, basal and intermediate snakes retain pelvic girdles and small rudiments of the femur. Moreover, legs may have re-emerged in extinct snake lineages [1–5], suggesting that the mechanisms of limb development were not completely lost in snakes. Here we report that hindlimb development arrests in python embryos as a result of mutations that abolish essential transcription factor binding sites in the limb-specific enhancer of *Sonic hedgehog* (*SHH*). Consequently, *SHH* transcription is weak and transient in python hindlimb buds, leading to early termination of a genetic circuit that drives limb outgrowth. Our results suggest that degenerate evolution of the *SHH* limb enhancer played a role in reduction of hindlimbs during snake evolution. By contrast, *HOXD* digit enhancers are conserved in pythons, and *HOXD* gene expression in the hindlimb buds progresses to the distal phase, forming an autopodial (digit) domain. Python hindlimb buds then develop transitory pre-chondrogenic condensations of the tibia, fibula, and footplate, raising the possibility that re-emergence of hindlimbs during snake evolution did not require de novo re-evolution of lost structures but instead could have resulted from persistence of embryonic legs.

RESULTS AND DISCUSSION

Disruption of the SHH/GREM1/AER-FGF Circuit by Early Arrest of *SHH* Transcription in Python Leg Buds

During snake evolution, pythons and boas diverged from the lineage leading to advanced snakes before hindlimbs were completely eliminated [6–8]. Python embryos initiate formation of hindlimb buds, but leg development is not sustained, resulting in formation of a rudimentary femur and terminal claw (Figure 1A). We showed previously that python hindlimb buds lack two critical signaling regions: the zone of polarizing activity (ZPA) and the apical ectodermal ridge (AER) [9]. The ZPA controls outgrowth and anteroposterior patterning of vertebrate limbs by secretion of Sonic hedgehog (SHH) protein [10, 11]. SHH protein was not detected in python hindlimb buds 1–2 days after oviposition [9], and others reported that the *cis*-regulatory element that directs limb-specific expression of *SHH* was lost in snakes [12, 13]. However, SHH can be activated in python hindlimb bud cells transplanted under the AER of chick wing buds [9], suggesting that the mechanism that controls *SHH* expression in limbs was not completely lost in pythons. To resolve this paradox, we first asked whether *SHH* transcription occurs in python hindlimb buds at stages earlier than those examined previously. In *Python regius* embryos harvested before oviposition and at stage 1 (the day of oviposition), *SHH* mRNA was detected in a small domain of cells at the posterior margin of the hindlimb buds, but this ZPA-like expression pattern is transient, disappearing within 24 hr of oviposition (Figures 1C and S1A). Analysis of hindlimb buds in comparably staged anole lizards (*Anolis sagrei*), which develop pentadactyl hindlimbs (Figure 1B), revealed a strong posterior domain of *shh* that persists after *SHH* becomes undetectable in python hindlimb buds (Figures 1C and 1D). To test whether weak and transient *SHH* expression in python hindlimbs results in hedgehog signal transduction, we examined expression of *PTCH1* and *GLI1*, two transcriptional readouts of SHH signaling [14]. *PTCH1* and *GLI1* are expressed in stage 1 python hindlimb buds (Figures 1E and 1G), but the expression domains are smaller and weaker than those observed in anoles (Figures 1F and 1H), and expression fades after termination of *SHH* expression (Figures 1E and 1G). In limbed tetrapods, *GLI3* is expressed anteriorly and distally in limb buds, where it regulates anteroposterior patterning of the digits by repressing *SHH* [15]. *GLI3* patterns are initially similar in python (stage 1) and anole (stage 5) hindlimb buds, showing strong anterior-distal expression that fades near the *SHH* domain, although at later stages, *GLI3* expression extends further proximally in pythons (Figures 1I and 1J). Thus, in python hindlimb buds, *SHH* transcription is initiated in a small group of posterior mesenchymal cells, and signal transduction occurs; however, *SHH* expression is transient, disappearing within 24 hr of oviposition.

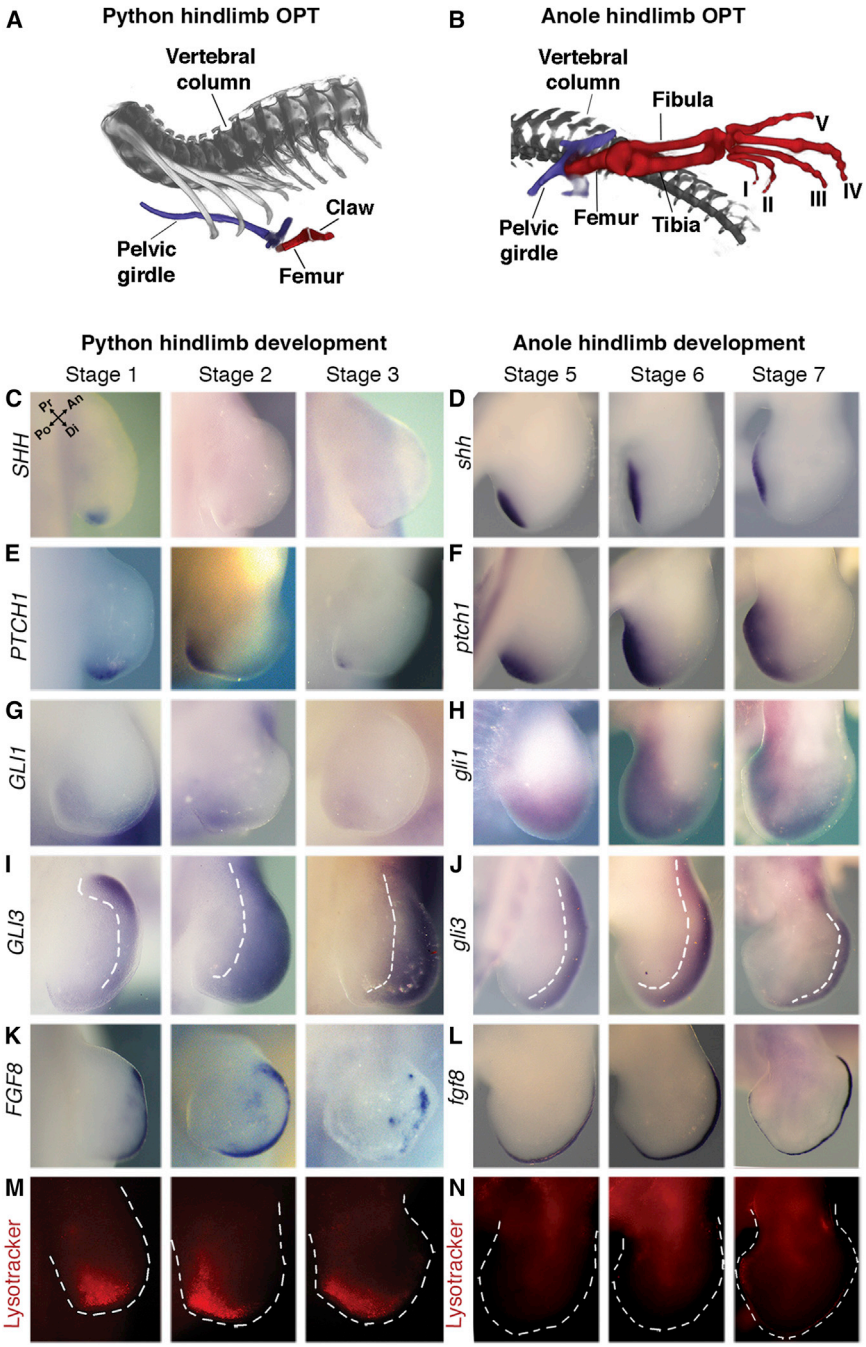

Figure 1. The *SHH/GREM1*/AER-*FGF* Circuit Is Activated but Not Maintained in Python Hindlimb Buds

(A and B) Optical projection tomography scans showing hindlimb skeletal anatomy in a ball python hatchling (A) and a stage 13 green anole lizard (B). The axial skeleton is shown in gray, pelvic girdle in blue, and hindlimb skeleton in red.

(C–L) Gene expression during hindlimb development in stage-matched python (C, E, G, I, and K) and anole (D, F, H, J, and L) embryos at three stages of development. Broken lines in (I) and (J) mark proximal limits of *GLI3* domains.

(M and N) Apoptosis in python (M) and anole (N) hindlimb buds stained with LysoTracker Red.

Black arrows in (C) indicate orientation of limb axes. An, anterior; Po, posterior; Pr, proximal; Di, distal. See also Figures S1 and S2.

Cessation of *SHH* transcription is followed by loss of target gene expression in the posterior region of python hindlimb buds.

SHH expression in vertebrate limbs is regulated in part by the AER, which secretes fibroblast growth factors (FGFs), and the dorsal ectoderm, which produces WNT7a [16–18]. We tested whether diminished activity of *SHH* in the python ZPA could result from deficiencies in either of these two ectodermal signaling regions. Analysis of *WNT7a* revealed dorsally compartmentalized expression in hindlimb ectoderm (Figure S1G), as occurs in other limbed tetrapods [16]. Together with our finding that LMX1 and EN1 are dorsoventrally restricted in python hindlimbs [9], this indicates the presence of a dorsal ectodermal signaling region and dorsoventral polarity in python hindlimb buds. In limbed tetrapods, AER cells along the distal edge of the limb buds undergo pseudostratification and produce FGFs, which maintain expression of *SHH* [17, 18]. SHH, in turn, feeds back to maintain expression of *FGF*s in the AER, establishing a positive feedback loop that coordinates limb outgrowth and patterning [19]. A morphological AER is evident in python hindlimb buds at stage 1 (Figures S2A and S2B), and *FGF8* is expressed in the AER before oviposition and at stage 1 (Figures 1K and S1B). Shortly after termination of *SHH*, the *FGF8* domain begins to degrade, disappearing from the posterior AER between stages 2 and 3, when weak and patchy expression can be detected anteriorly (Figure 1K). The posterior-to-anterior loss of *FGF8* in python hindlimb buds coincides with the posterior-to-anterior flattening of the AER (Figures S2C –S2E). The changes in python AER structure and *FGF8* expression resemble those seen in mouse hindlimb buds after early deletion of *Shh* [11], although the severity of ridge degeneration is greater in pythons, possibly reflecting disruption of factors in addition to SHH. Anole hindlimb buds, by contrast, maintain a pronounced AER that expresses *Fgf8* throughout (Figure 1L).

In limbed tetrapods, SHH maintains the AER by inducing *Gremlin1* (*GREM1*), which counteracts the inhibitory activity of bone morphogenetic proteins (BMPs) on the AER [20]. *GREM1* is expressed throughout the anteroposterior axis of the python hindlimb bud at stage 1 but then weakens following loss of *SHH* (Figure S1I). By contrast, expression of *BMP4* and its target

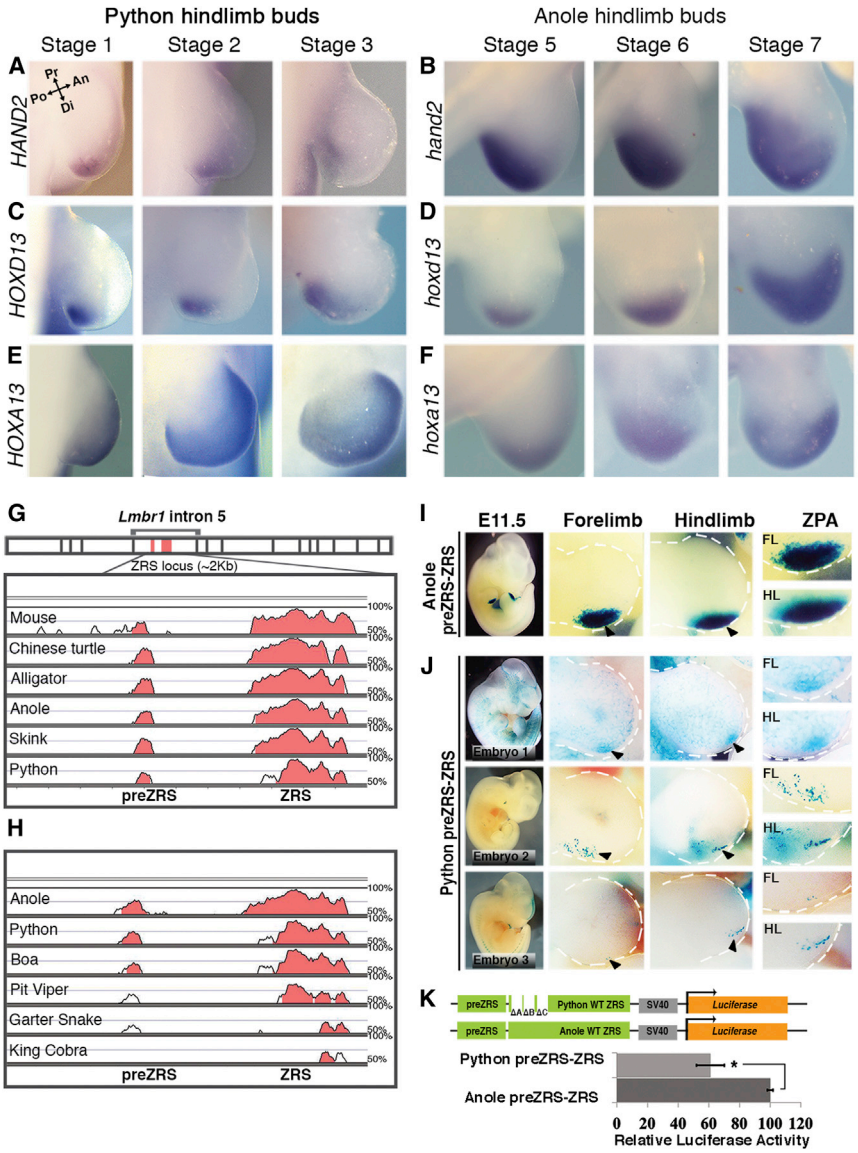

Figure 2. Analysis of *trans*- and *cis*-Regulators of *SHH* Reveals Degeneration and Hypofunctionalization of the Python ZRS

(A–F) Expression of *HAND2* (A and B), *HOXD13* (C and D), and *HOXA13* (E and F) in stage-matched hindlimb buds of python (A, C, and E) and anole (B, D, and F) embryos.

(G and H) VISTA conservation plots using human reference sequence to compare architecture of the ZRS locus. Peaks indicate conservation > 50%, and colored peaks indicate conservation > 75%. (G) Comparison of ZRS locus conservation in python, limbed reptiles, and mouse. (H) Intra-squamate comparison of ZRS locus conservation in python, boa, three completely limbless advanced snakes, and anole lizard.

(I and J) Functional analysis of preZRS-ZRS enhancers from anole (I) and python (J) in transgenic mice. Columns show, from left to right, whole embryos at E11.5, forelimb buds, hindlimb buds, and high-magnification views of the ZPA in forelimb (FL) and hindlimb (HL) buds. (I) Anole preZRS-ZRS drove strong LacZ expression in ZPA of forelimbs and hindlimbs. (J) Three examples of transgenic mouse embryos with the python preZRS-ZRS construct showing weak reporter activity in forelimbs and hindlimbs. See Experimental Procedures for sample sizes.

(K) Quantification of python and anole PreZRS-ZRS activity in a luciferase reporter assay demonstrates that the python enhancers have reduced transcriptional regulatory activity (asterisk indicates significant difference in two-tailed t test, $n = 4$, $p = 1.6 \times 10^{-4}$). Error bars indicate standard deviations.

See also Figure S4.

gene, *MSX2*, is sustained in the distal mesenchyme from stages 1 to 3 (Figures S1J and S1K). In chick limbs, FGF signaling from the AER drives distal limb development, in part, by regulating cell survival [21, 22]. Comparison of apoptotic patterns in hindlimb buds of stage-matched python and anole embryos revealed a posterior-distal domain of apoptosis in pythons that was not observed in anoles (Figures 1M and 1N). As the python AER degenerates during stages 2 and 3, the apoptotic domain expands distally (Figure 1M), consistent with loss of AER signaling activity. Together, these results indicate that after the transient pulse of *SHH* expression at stage 1, the SHH/GREM1/AER-FGF feedback loop breaks down in python hindlimb buds.

Degenerate Evolution of the Python ZRS Underlies Diminished Transcription of *SHH*

Transcription of *SHH* in tetrapod limbs is activated by binding of transcription factors to a *cis*-regulatory element known as the ZPA Regulatory Sequence (ZRS), a limb-specific enhancer located ~1 Mb upstream of *SHH*, in intron 5 of the *LMBR1* gene [23–26]. We first asked whether the arrest of *SHH* transcription in python hindlimbs is associated with disruption of *trans*-acting regulators of the ZRS. *HAND2*, *HOXD13*, and *HOXA13*, which encode proteins that bind the ZRS in mice [23–25, 27], showed strikingly similar expression patterns in early hindlimb buds of python (pre-oviposition and stage 1) and anole (stage 5) embryos (Figures 2A–2F, S1C, and S1D). After the loss of *SHH* expression in python hindlimb buds, *HAND2* expression became progressively weaker (stages 2 and 3 in Figure 2A), consistent with the finding that SHH maintains *Hand2* posteriorly in mice [28, 29]. *HOXA13* and *HOXD13* expression persists distally in python (stages 2 and 3) and anole (stages 6 and 7) hindlimbs (Figures 2C–2F). Although species-specific differences were observed after the loss of *SHH* in pythons, *HAND2*, *HOXD13*, and *HOXA13* expression were highly conserved in early python and anole hindlimb buds.

We next asked whether diminished *SHH* expression in python hindlimb buds could reflect changes to the integrity of the python ZRS. Cloning of the ~9 kb intron 5 of *LMBR1* showed that, in contrast to previous reports that the ZRS has been lost in snakes [13], pythons have a conserved region that corresponds to the

ZRS of limbed tetrapods (Figure 2G). We also identified a conserved preZRS, an additional *SHH* limb enhancer near the ZRS [30] (Figure 2G). Comparative genomic analysis showed that despite an overall high degree of similarity in the ZRS and preZRS sequences in pythons and limbed amniotes, the 5′ end of python ZRS contains a region of divergence (Figure 2G), raising the possibility that mutations in the ZRS could play a role in diminished activity of *SHH* in pythons.

We then compared preZRS-ZRS sequences from anole, python, boa (*Boa constrictor*, a boid), pit viper (*Prothobothrops mucrosquamatus*, a viperid), garter snake (*Thamnophis sirtalis*, a colubrid), and king cobra (*Ophiophagus hannah*, an elapid). The results show a pattern of degenerative evolution in which advanced snakes (pit viper, garter snake, and king cobra), which are completely limbless, show significantly less conservation of the preZRS and the ZRS than either python or boa, which retain limb rudiments (Figure 2H). Python and boa have nearly identical patterns of sequence conservation in the preZRS and the ZRS, with each showing limited divergence at the 5′ end of the ZRS (Figure 2H). Pit viper and garter snake showed less conservation of the preZRS and the ZRS when compared to python and boa. The pattern of preZRS conservation was similar in pit viper and garter snake, but garter snake ZRS showed marked divergence (Figure 2H). King cobra showed the most extreme degradation of both enhancers; there was no signature of a preZRS and only limited conservation at the 3′ end of the ZRS (Figure 2H).

In order to determine the effects of python ZRS sequence divergence on its regulatory activity, we generated LacZ reporter constructs containing the python preZRS-ZRS (preZRS-ZRS-LacZ) and examined their activity in transgenic mice. A second reporter construct containing the anole preZRS-ZRS was generated as a squamate control. The anole preZRS-ZRS drives transcription in a strong ZPA-like domain in mouse forelimbs and hindlimbs at embryonic day 11.5 (Figure 2I). In contrast, the python preZRS-ZRS showed minimal activity in mouse forelimbs and hindlimbs, with patterns ranging from a small number of LacZ-positive cells to no detectable activity (Figure 2J). To quantify differences in the regulatory activity of the python and anole preZRS-ZRS, we cloned each enhancer into a luciferase reporter vector and transfected them into mouse fibroblasts (Figure 2K). Python preZRS-ZRS showed a 40% reduction in luciferase transcriptional activation compared to the anole preZRS-ZRS (Figure 2K). Thus, in vivo and in vitro analyses show that python preZRS-ZRS is a weak driver of transcription, raising the possibility that divergence of the 5′ end of this enhancer underlies diminished *SHH* expression in python hindlimb buds.

The ZRS is divisible into two domains with different regulatory roles. The 5′ end carries spatiotemporal (ZPA-specific) regulatory information, whereas the 3′ end regulates long-range interaction with the *SHH* promoter [31]. Transcriptional regulators of *SHH* in the mouse ZPA, such as HAND2 and posterior HOXD proteins, bind to the 5′ end of the ZRS domain [23–25]. We characterized the divergent sequence at the 5′ end of the python ZRS and identified three major deletions (ΔA, ΔB, and ΔC) not found in limbed amniotes (Figure 3A). The three deletions are shared by three python species (*P. regius*, *P. molurus*, and *P. reticulatus*) and a boid (*Boa constrictor*), indicating their presence in the last common ancestor of Pythonidae and Boidae.

To determine how each mutation in the python ZRS affects its activity, we used site-directed mutagenesis to introduce the mutations individually (ΔA, ΔB, or ΔC) and together (ΔABC) into the mouse preZRS-ZRS sequence and then cloned these into a luciferase reporter construct to assay their activities in cell culture (Figure S3A). Comparison of the activity of the python ZRS deletion constructs and a WT mouse ZRS control construct showed that each of the three python deletions caused a reduction of luciferase activity, with ΔC causing the largest decrease (19.6% of control activity level), followed by ΔA (53.2%) and ΔB (78.8%) (Figure 3B). The ZRS bearing all three python deletions (ΔABC) decreased luciferase activity to 12.8% of the WT control level, a level lower than any of the three individual deletions (Figure 3B). If the activity that we observed in vitro is representative of the endogenous effects of these deletions, then the results suggest that each of the three mutations could have reduced the efficiency of the ZRS during snake evolution and that these effects were likely cumulative.

Mutations in Python ZRS Disrupt HOXD Binding Sites Required for Enhancer Activation

We next investigated the mechanism by which the ΔA, ΔB, and ΔC mutations cause reductions in python ZRS activity. In mouse limbs, the ZRS is transactivated by HAND2, ETS1, and HOXD proteins [23–25, 32]. HAND2 and ETS1 binding sites have been characterized at the nucleotide level in mice, and analysis of these sites in the python ZRS revealed that the HAND2 binding site is not disrupted but that one of the five ETS1 binding sites was eliminated (Figure S4). Because the precise positions at which HOXD proteins bind the 5′ end of the mouse ZRS are less well understood, it was unclear how the python ZRS mutations affect its transactivation by HOXD9, HOXD10, or HOXD13. We addressed this by co-transfecting mouse fibroblasts with a WT mouse preZRS-ZRS construct or a mouse preZRS-ZRS construct bearing the python ZRS mutations individually (ΔA, ΔB, or ΔC) or together (ΔABC), along with *Hoxd9*, *Hoxd10*, or *Hoxd13* expression vectors. The WT mouse preZRS-ZRS construct showed greatest transactivation by HOXD13 (7.6-fold), followed by HOXD9 (3.7-fold) and then HOXD10 (1.2-fold) (Figures 3C and S3B). When python ZRS deletion constructs with mutations ΔA, ΔB, ΔC, or ΔABC were co-transfected with *Hoxd9*, *Hoxd10*, or *Hoxd13*, each of the python deletion constructs showed reduced transactivation relative to the mouse control (Figures 3C, 3D, and S3B). Transactivation was weakest in the ZRS bearing all three python mutations. For example, when co-transfected with *Hoxd9*, *Hoxd10*, and *Hoxd13* expression vectors, the python ΔABC-ZRS construct showed only 2% of the activity of the control mouse ZRS that lacked these mutations (Figures 3C). Thus, each mutation in the python ZRS weakens its response to HOXD proteins, and all three mutations virtually abolish HOXD transactivation of the python ZRS.

The results described above suggested that HOXD binding sites were disrupted during evolution of the python ZRS. To test this hypothesis directly, we asked whether HOXD13, HOXD10, and HOXD9 can bind to the ~400 bp region at the 5′ end of the mouse ZRS that corresponds to the domain containing the three python deletions. Electrophoretic mobility shift assays (EMSAs) show that all three HOXD proteins bind to this region of the mouse ZRS (Figure S3C). To determine whether python

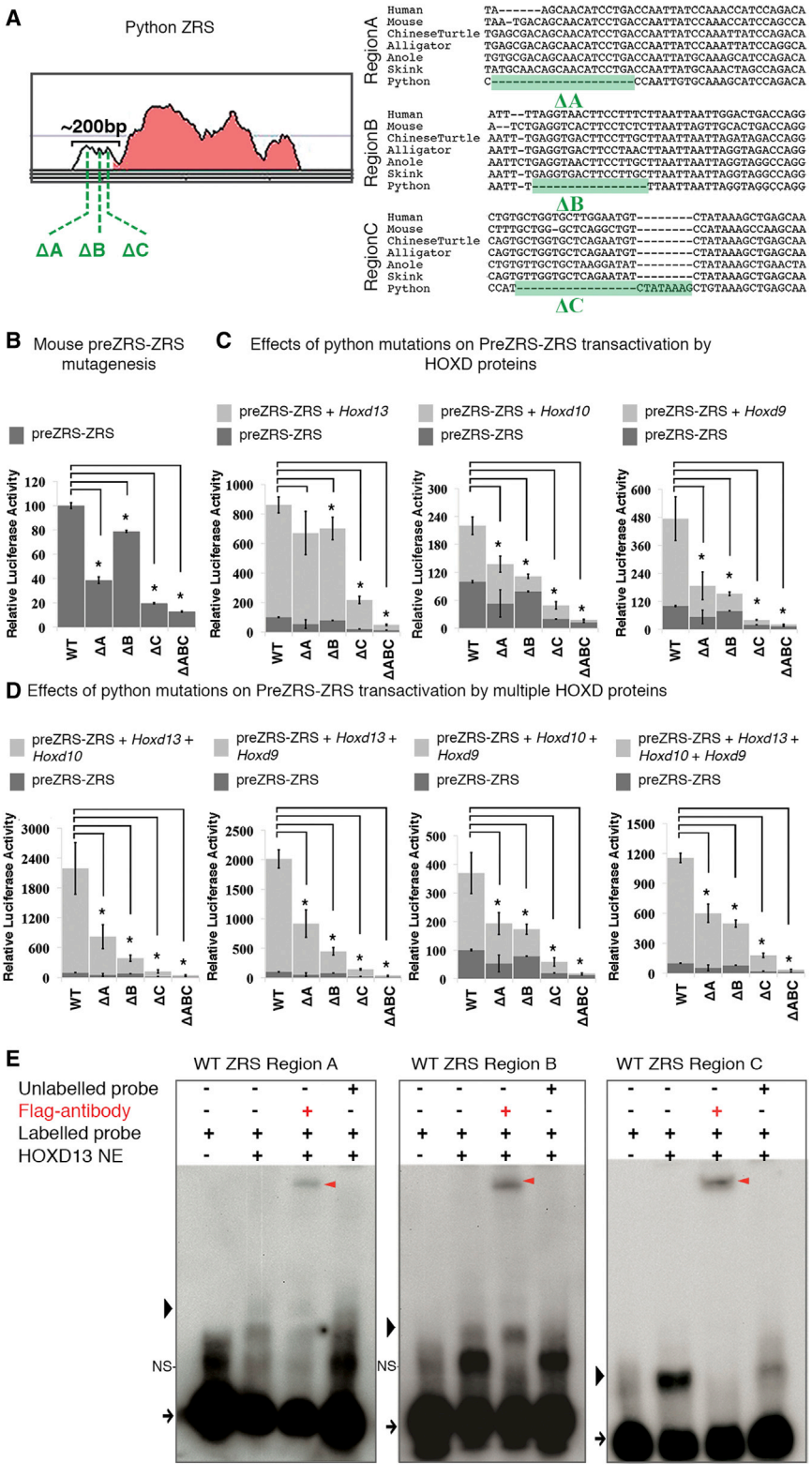

Figure 3. Molecular Evolution of the Python ZRS: Loss of Three Binding Sites Abolishes Transactivation by HOXD Proteins

(A) The 5′ end of the python ZRS shows three specific deletions, ΔA, ΔB, and ΔC (ΔC also has an 8 nt microduplication). These mutations are conserved in three python and one boid species (also see Figure S4).

(B–D) Luciferase reporter analyses of mouse preZRS-ZRS constructs harboring python deletions individually (ΔA, ΔB, or ΔC) and together (ΔABC). Asterisks indicate significant differences, two-tailed t test, n = 4. Error bars indicate standard deviations. See Figure S3B for numerical data and p values. (B) Effects of python deletions on ZRS activity. (C) Effects of python mutations on ZRS transactivation by HOXD13, HOXD10, and HOXD9. (D) Effects of python mutations on ZRS transactivation by different combinations of HOXD13, HOXD10, and HOXD9.

(E) HOXD13-3xFlag binds WT control ZRS regions that correspond to the deleted regions in the python ZRS (see Supplemental Experimental Procedures for oligonucleotide sequences). Each oligonucleotide corresponds to WT mouse sequence at positions equivalent to each python deletion (ΔA in region A, ΔB in region B, ΔC in region C).

NE, nuclear extracts; NS, non-specific band; black arrowheads, shifts; red arrowheads, supershifts. See also Figures S3 and S4.

ZRS mutations ΔA, ΔB, or ΔC reside in a region necessary for HOXD binding, we designed three short (40 nt) oligonucleotides from regions of the mouse ZRS that were deleted by mutations A, B, and C in pythons (Figure S4). Only HOXD13 binds all three oligonucleotides (Figure 3E), suggesting that python ZRS mutations A, B, and C each occurred in HOXD13 binding sites and that its synergy with HOXD9 and HOXD10 could be mediated by protein-protein interactions rather than by direct binding of HOXD10 or HOXD9 to these regions of the ZRS. These findings, together with results from our functional studies of each python ZRS mutation, show that python mutations ΔA, ΔB, and ΔC each removed a HOXD13 binding site that is essential for transactivation of the ZRS. Thus, by abolishing sites required for binding of HOXD13, the mutations at the 5′ end of the ZRS can account for the diminished transcription of *SHH* in python hindlimb buds.

Conservation of the Distal *HOXD* Regulatory Landscape and Autopodial Development in Pythons

Despite the premature breakdown of the SHH/GREM1/AER-FGF feedback loop in python hindlimb buds, our analysis of HOX gene expression suggested the onset of a late/distal phase of *HOXD13* expression at stage 3 (Figure 2C). In light of the relationship between distal expression of *HOX13* paralogs and digit development in

limbed tetrapods, we monitored the progression of *HOXD13* and *HOXA13* in python hindlimb buds at later stages. Surprisingly, *HOXD13* expression spread throughout the distal region of the python hindlimb bud, overlapping with *HOXA13* expression in a pattern that resembles the autopodial (digit-forming) domains of *HOXD13* and *HOXA13* in limbed tetrapods (Figures 4A and 4B) [33, 34]. This late/distal phase of *HOXD13* expression was unexpected given the absence of any remnant of a foot in pythons.

In mice, distal limb expression of *Hoxd13* is controlled by a series of enhancers in a Topologically Associating Domain (TAD) centromeric to the *HOXD* cluster [35]. Analysis of the syntenic region in python revealed striking conservation of the distal limb and genital enhancer sequences (Prox, CsA, CsB, and I-V regulatory islands) that regulate *HOXD* expression during tetrapod digit and external genital development (Figure 4F). The presence of distal *HOXD* enhancers and the autopod-like patterns of *HOXD13* and *HOXA13* expression in python hindlimb buds prompted us to look for evidence of distal hindlimb skeletogenesis. Analysis of *SOX9* expression, which marks pre-chondrogenic skeletal condensations, revealed a Y-shaped domain in the proximal and middle region of the hindlimb and a distal domain that overlaps with the distal region of *HOXD13* and *HOXA13* expression at stages 4 and 5/6 (Figures 4A–4C). Over the next two stages, *SOX9* expression in python hindlimbs delineates discrete skeletal condensations that resemble the three major segments (zeugopod, stylopod, and autopod) of the tetrapod limb (Figure 4D). Comparison of the *SOX9* domains in python in anole hindlimbs suggests that the python condensations could be anlagen of the femur, tibia and fibula, and digital plate (Figures 4D and 4E). The fate of these zeugopodial and autopodial skeletal condensations is unknown, but they are transitory structures, as distal hindlimb elements are not found in mature pythons. Taken together, our results show that pythons have accumulated degenerative mutations in the ZRS that cause precocious arrest of *SHH* expression in hindlimb buds, whereas *HOXD* digit- and genital-specific enhancers have been maintained in pythons, and this likely underlies the distal activation of *HOXD13* and perhaps the specification of distal skeletal elements in python hindlimb buds.

Conclusions

The results presented here suggest that diminished expression of *SHH* in the early limb buds of python embryos is a consequence of three mutations (ΔA, ΔB, and ΔC) in the 5′ end of the ZRS that disrupt sites required for ZRS transactivation by HOXD proteins. We note that our analysis also uncovered a deletion of a single ETS1 binding site in the ZRS, and although loss of a single ETS1 site is not sufficient to alter ZRS activity in mice [32], we cannot exclude a role for this deletion in the diminished activity of the python ZRS. Our identification of the same three mutations in the ZRS of pythons and boas indicates that ΔA, ΔB, and ΔC were present in their last common ancestor (Figure 4G). Based on recent calibrations of the python and boid clades [6–8], all three mutations likely arose by the late Upper Cretaceous, when snakes underwent a major adaptive radiation [1–5, 7, 8]. We propose that divergence of the ZRS sequence during snake evolution initially rendered the enhancer hypofunctional, compromising its ability to drive *SHH* transcription and, ultimately, resulting in cessation of hindlimb outgrowth and loss of distal structures (Figure 4G). Furthermore, our observation that mutations ΔA, ΔB, and ΔC have cumulative effects on ZRS activity suggests that increased sequence divergence could have resulted in progressive reduction of the hindlimb skeleton in basal and intermediate snakes. Hindlimbs disappeared completely in advanced snakes (caenophidians), and comparison of preZRS-ZRS structure across snakes revealed a pattern of degenerative evolution affecting the preZRS and the ZRS in vipers, colubrids, and elapids. Furthermore, only the 3′ end of the ZRS is conserved among all snake taxa examined here, suggesting that ZRS degradation began at the 5′ end. Conservation at the 3′ end of the ZRS in limbless snakes raises questions about the significance of this region outside the context of limb development.

Despite the accumulation of mutations in the ZRS and the reduced nature of python hindlimbs, the genomic and transcriptional machinery necessary to develop limbs has been largely conserved, from the genetic circuitry active in early limb buds to the specification of an autopodial (toe-forming) domain. Conservation of *HOXD* enhancers centromeric to the *HOXD* cluster in snakes suggests that this regulatory domain remained under selection after its role in digit development became obsolete. Our recent finding that *HOXD* genes, but not *SHH*, are transcribed in the developing hemipenes of pythons [36], together with evidence that *HOXD* expression in digits and external genitalia are under shared regulatory control [37], suggests that the *HOXD* distal enhancers were retained in snakes due to their essential role in external genital development. Finally, our discovery that python embryos develop transitory cartilage condensations of the lower leg and foot suggests that re-acquisition of fully developed hindlimbs in extinct snakes [1–5] may not have required de novo re-evolution of lost structures, but could have resulted from persistence of the embryonic legs.

EXPERIMENTAL PROCEDURES

Animal protocols were reviewed and approved by the University of Florida Institutional Animal Care and Use Committee. Full experimental procedures can be found in the Supplemental Experimental Procedures.

ACCESSION NUMBERS

The accession numbers for the sequences reported in this paper are GenBank: KX778812-KX778839 and KX824111-KX824112.

SUPPLEMENTAL INFORMATION

Supplemental Information includes Supplemental Experimental Procedures and four figures and can be found with this article online at http://dx.doi.org/10.1016/j.cub.2016.09.020.

A video abstract is available at http://dx.doi.org/10.1016/j.cub.2016.09.020#mmc3.

AUTHOR CONTRIBUTIONS

F.L. and M.J.C. designed the experiments. F.L. performed the experiments. F.L. and M.J.C. analyzed the data, interpreted the results, and wrote the manuscript.

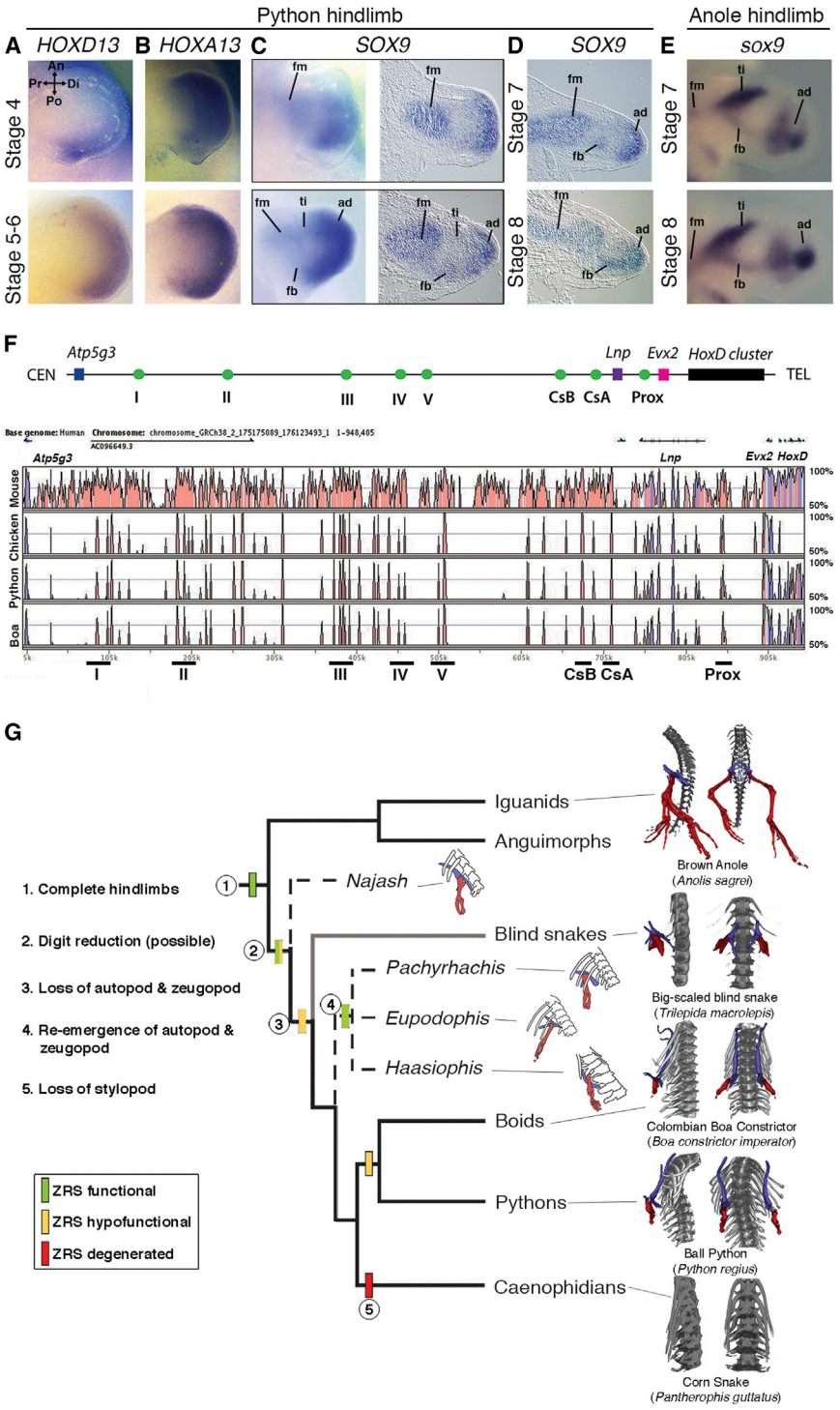

Figure 4. ZRS Degeneration and Cryptic Hindlimb Development in Python Embryos Suggests a Model for Loss and Re-acquisition of Legs during Snake Evolution

(A and B) Python hindlimb buds exhibit a late distal autopodial phase of *HOXD13* and *HOXA13* expression.

(C–E) *SOX9* expression delineates prechondrogenic condensations in three discrete regions (stylopod, zeugopod, and autopod) of stage-matched python (C and D) and anole (E) hindlimbs. Note that *SOX9* distal domain develops within the autopodial domain of *HOXD13*/*HOXA13* expression in python (compare A and B with C and D). fm, femur; fb fibula; ad, autopodial domain. Black arrows show limb axes: An, anterior; Pr, proximal; Di, distal; Po, posterior.

(F) VISTA conservation plots (using human sequence as reference) show that python and boa retain the conserved regulatory archipelago of *HOXD* digit and genital enhancers in the gene desert centromeric to the *HOXD* cluster. Peaks indicate the presence of conserved sequences A (CsA) and CsB of the Global Control Region, Prox, and the five regulatory islands.

(G) Model for the role of degenerate evolution of the ZRS in snake hindlimb reduction. Phylogeny adapted from [3, 5, 6, 8]. Hindlimb structures (red) shown at right were generated by optical projection tomography (except for fossil species). ZRS is indicated by green (functional), yellow (hypofunctional), or red (degenerated); solid outlines indicate known ZRS status; broken outlines indicate predicted status. Tree branches are black for lineages with known ZRS structure, gray for predicted structure, and broken for extinct lineages. (1) Ancestral ZRS (green) drove *SHH* expression and digit development in limbed squamates. (2) We propose that after the divergence of *Serpentes* from limbed squamates, mutations ΔA, ΔB, and ΔC weakened ZRS function (yellow), reducing *SHH* activity and causing loss of distal hindlimb elements. Yellow/green ZRS reflects uncertainty about whether digit reduction occurred in the fossil *Najash* or whether absence of digits reflects taphonomic conditions. (3) Absence of a tibia, fibula, foot, and toes in scolecophidians (e.g., blind snakes) and alethinophidians suggests ZRS hypofunctionalization in the common ancestor. Transitory prechondrogenic condensations of zeugopodial and autopodial skeleton form in embryos but then degenerate, resulting in absence of these structures in adults. (4) Re-emergence of the tibia and fibula (zeugopod) and digits (autopod) in Tethyan snakes may have resulted from persistence of embryonic skeletal condensations into adulthood. The requirement of the ZRS for digit development suggests that ZRS activity may have been amplified, despite the presence of deletions. (5) Further degeneration of the ZRS (red) in advanced snakes (caenophidians) rendered it non-functional (see Figure 2H), resulting in total limblessness. Skeletal morphologies pictured next to the tree terminals were derived from OPT scans, except for fossil species.

ACKNOWLEDGMENTS

We are grateful to K. Kelley and K. Backer-Kelley at the UF ICBR electron microscopy core for assistance with SEM; J. Wisby, B. Cole, O. Tarazona, B. Caruso, T. Sanger, and B. Kircher for assistance with animal husbandry and/or eggs; B. Cole and Colección Herpetológica Universidad Industrial de Santander (UISR-2549) for adult snake material; R. Renne and H.-S. Choi for help with luciferase assays; and C. Larkins and D. Menke for sharing materials. F.L. thanks the Gans Collections and Charitable Fund. This project was supported the Howard Hughes Medical Institute (M.J.C). F.L. is an HHMI international student research fellow.

Received: July 14, 2016
Revised: August 29, 2016
Accepted: September 12, 2016
Published: October 20, 2016

REFERENCES

1. Caldwell, M.W., and Lee, M.S.Y. (1997). A snake with legs from the marine Cretaceous of the Middle East. Nature *386*, 705–709.
2. Rage, J.C., and Escuillié, F. (2000). Un nouveau serpent bipède du Cénomanien (Crétacé). Implications phylétiques. C. R. Acad. Sci. Paris Earth Sci. *330*, 513–520.
3. Houssaye, A., Xu, F., Helfen, L., Buffrénil, V.D., Baumbach, T., and Tafforeau, P. (2011). Three-Dimensional Pelvis and Limb Anatomy of the Cenomanian Hind-Limbed Snake Eupodophis descouensi (Squamata, Ophidia) Revealed by Synchrotron-Radiation Computed Laminography. J. Vertebr. Paleontol. *31*, 2–7.
4. Tchernov, E., Rieppel, O., Zaher, H., Polcyn, M.J., and Jacobs, L.L. (2000). A fossil snake with limbs. Science *287*, 2010–2012.
5. Apesteguía, S., and Zaher, H. (2006). A Cretaceous terrestrial snake with robust hindlimbs and a sacrum. Nature *440*, 1037–1040.
6. Pyron, R.A., Burbrink, F.T., and Wiens, J.J. (2013). A phylogeny and revised classification of Squamata, including 4161 species of lizards and snakes. BMC Evol. Biol. *13*, 93.
7. Head, J.J. (2015). Fossil calibration dates for molecular phylogenetic analysis of snakes 1: Serpentes, Alethinophidia, Boidae, Pythonidae. Palaeontol. Electronica *18.1.6FC*, 1–17.
8. Zheng, Y., and Wiens, J.J. (2016). Combining phylogenomic and supermatrix approaches, and a time-calibrated phylogeny for squamate reptiles (lizards and snakes) based on 52 genes and 4162 species. Mol. Phylogenet. Evol. *94* (Pt B), 537–547.
9. Cohn, M.J., and Tickle, C. (1999). Developmental basis of limblessness and axial patterning in snakes. Nature *399*, 474–479.
10. Riddle, R.D., Johnson, R.L., Laufer, E., and Tabin, C. (1993). Sonic hedgehog mediates the polarizing activity of the ZPA. Cell *75*, 1401–1416.
11. Zhu, J., Nakamura, E., Nguyen, M.-T., Bao, X., Akiyama, H., and Mackem, S. (2008). Uncoupling Sonic hedgehog control of pattern and expansion of the developing limb bud. Dev. Cell *14*, 624–632.
12. Sagai, T., Hosoya, M., Mizushina, Y., Tamura, M., and Shiroishi, T. (2005). Elimination of a long-range cis-regulatory module causes complete loss of limb-specific Shh expression and truncation of the mouse limb. Development *132*, 797–803.
13. Sagai, T., Masuya, H., Tamura, M., Shimizu, K., Yada, Y., Wakana, S., Gondo, Y., Noda, T., and Shiroishi, T. (2004). Phylogenetic conservation of a limb-specific, cis-acting regulator of Sonic hedgehog (Shh). Mamm. Genome *15*, 23–34.
14. Pearse, R.V., 2nd, Vogan, K.J., and Tabin, C.J. (2001). Ptc1 and Ptc2 transcripts provide distinct readouts of Hedgehog signaling activity during chick embryogenesis. Dev. Biol. *239*, 15–29.
15. Büscher, D., Bosse, B., Heymer, J., and Rüther, U. (1997). Evidence for genetic control of Sonic hedgehog by Gli3 in mouse limb development. Mech. Dev. *62*, 175–182.
16. Yang, Y., and Niswander, L. (1995). Interaction between the signaling molecules WNT7a and SHH during vertebrate limb development: dorsal signals regulate anteroposterior patterning. Cell *80*, 939–947.
17. Laufer, E., Nelson, C.E., Johnson, R.L., Morgan, B.A., and Tabin, C. (1994). Sonic hedgehog and Fgf-4 act through a signaling cascade and feedback loop to integrate growth and patterning of the developing limb bud. Cell *79*, 993–1003.
18. Niswander, L., Tickle, C., Vogel, A., Booth, I., and Martin, G.R. (1993). FGF-4 replaces the apical ectodermal ridge and directs outgrowth and patterning of the limb. Cell *75*, 579–587.
19. Niswander, L., Jeffrey, S., Martin, G.R., and Tickle, C. (1994). A positive feedback loop coordinates growth and patterning in the vertebrate limb. Nature *371*, 609–612.
20. Scherz, P.J., Harfe, B.D., McMahon, A.P., and Tabin, C.J. (2004). The limb bud Shh-Fgf feedback loop is terminated by expansion of former ZPA cells. Science *305*, 396–399.
21. Rowe, D.A., Cairns, J.M., and Fallon, J.F. (1982). Spatial and temporal patterns of cell death in limb bud mesoderm after apical ectodermal ridge removal. Dev. Biol. *93*, 83–91.
22. Fallon, J.F., López, A., Ros, M.A., Savage, M.P., Olwin, B.B., and Simandl, B.K. (1994). FGF-2: apical ectodermal ridge growth signal for chick limb development. Science *264*, 104–107.
23. Galli, A., Robay, D., Osterwalder, M., Bao, X., Bénazet, J.D., Tariq, M., Paro, R., Mackem, S., and Zeller, R. (2010). Distinct roles of Hand2 in initiating polarity and posterior Shh expression during the onset of mouse limb bud development. PLoS Genet. *6*, e1000901.
24. Osterwalder, M., Speziale, D., Shoukry, M., Mohan, R., Ivanek, R., Kohler, M., Beisel, C., Wen, X., Scales, S.J., Christoffels, V.M., et al. (2014). HAND2 targets define a network of transcriptional regulators that compartmentalize the early limb bud mesenchyme. Dev. Cell *31*, 345–357.
25. Capellini, T.D., Di Giacomo, G., Salsi, V., Brendolan, A., Ferretti, E., Srivastava, D., Zappavigna, V., and Selleri, L. (2006). Pbx1/Pbx2 requirement for distal limb patterning is mediated by the hierarchical control of Hox gene spatial distribution and Shh expression. Development *133*, 2263–2273.
26. Lettice, L.A., Heaney, S.J., Purdie, L.A., Li, L., de Beer, P., Oostra, B.A., Goode, D., Elgar, G., Hill, R.E., and de Graaff, E. (2003). A long-range Shh enhancer regulates expression in the developing limb and fin and is associated with preaxial polydactyly. Hum. Mol. Genet. *12*, 1725–1735.
27. Johnson, E.J., Neely, D.M., Dunn, I.C., and Davey, M.G. (2014). Direct functional consequences of ZRS enhancer mutation combine with secondary long range SHH signalling effects to cause preaxial polydactyly. Dev. Biol. *392*, 209–220.
28. Charité, J., McFadden, D.G., and Olson, E.N. (2000). The bHLH transcription factor dHAND controls Sonic hedgehog expression and establishment of the zone of polarizing activity during limb development. Development *127*, 2461–2470.
29. Litingtung, Y., Dahn, R.D., Li, Y., Fallon, J.F., and Chiang, C. (2002). Shh and Gli3 are dispensable for limb skeleton formation but regulate digit number and identity. Nature *418*, 979–983.
30. Park, K., Kang, J., Subedi, K.P., Ha, J.H., and Park, C. (2008). Canine polydactyl mutations with heterogeneous origin in the conserved intronic sequence of LMBR1. Genetics *179*, 2163–2172.
31. Lettice, L.A., Williamson, I., Devenney, P.S., Kilanowski, F., Dorin, J., and Hill, R.E. (2014). Development of five digits is controlled by a bipartite long-range cis-regulator. Development *141*, 1715–1725.
32. Lettice, L.A., Williamson, I., Wiltshire, J.H., Peluso, S., Devenney, P.S., Hill, A.E., Essafi, A., Hagman, J., Mort, R., Grimes, G., et al. (2012). Opposing functions of the ETS factor family define Shh spatial expression in limb buds and underlie polydactyly. Dev. Cell *22*, 459–467.
33. Nelson, C.E., Morgan, B.A., Burke, A.C., Laufer, E., DiMambro, E., Murtaugh, L.C., Gonzales, E., Tessarollo, L., Parada, L.F., and Tabin, C. (1996). Analysis of Hox gene expression in the chick limb bud. Development *122*, 1449–1466.
34. Zakany, J., and Duboule, D. (2007). The role of Hox genes during vertebrate limb development. Curr. Opin. Genet. Dev. *17*, 359–366.
35. Montavon, T., Soshnikova, N., Mascrez, B., Joye, E., Thevenet, L., Splinter, E., de Laat, W., Spitz, F., and Duboule, D. (2011). A regulatory archipelago controls Hox genes transcription in digits. Cell *147*, 1132–1145.
36. Leal, F., and Cohn, M.J. (2015). Development of hemipenes in the ball python snake Python regius. Sex Dev. *9*, 6–20.
37. Lonfat, N., Montavon, T., Darbellay, F., Gitto, S., and Duboule, D. (2014). Convergent evolution of complex regulatory landscapes and pleiotropy at Hox loci. Science *346*, 1004–1006.

Current Biology, Volume *26*

Supplemental Information

Loss and Re-emergence of Legs in Snakes by Modular Evolution of *Sonic hedgehog* and *HOXD* Enhancers

Francisca Leal and Martin J. Cohn

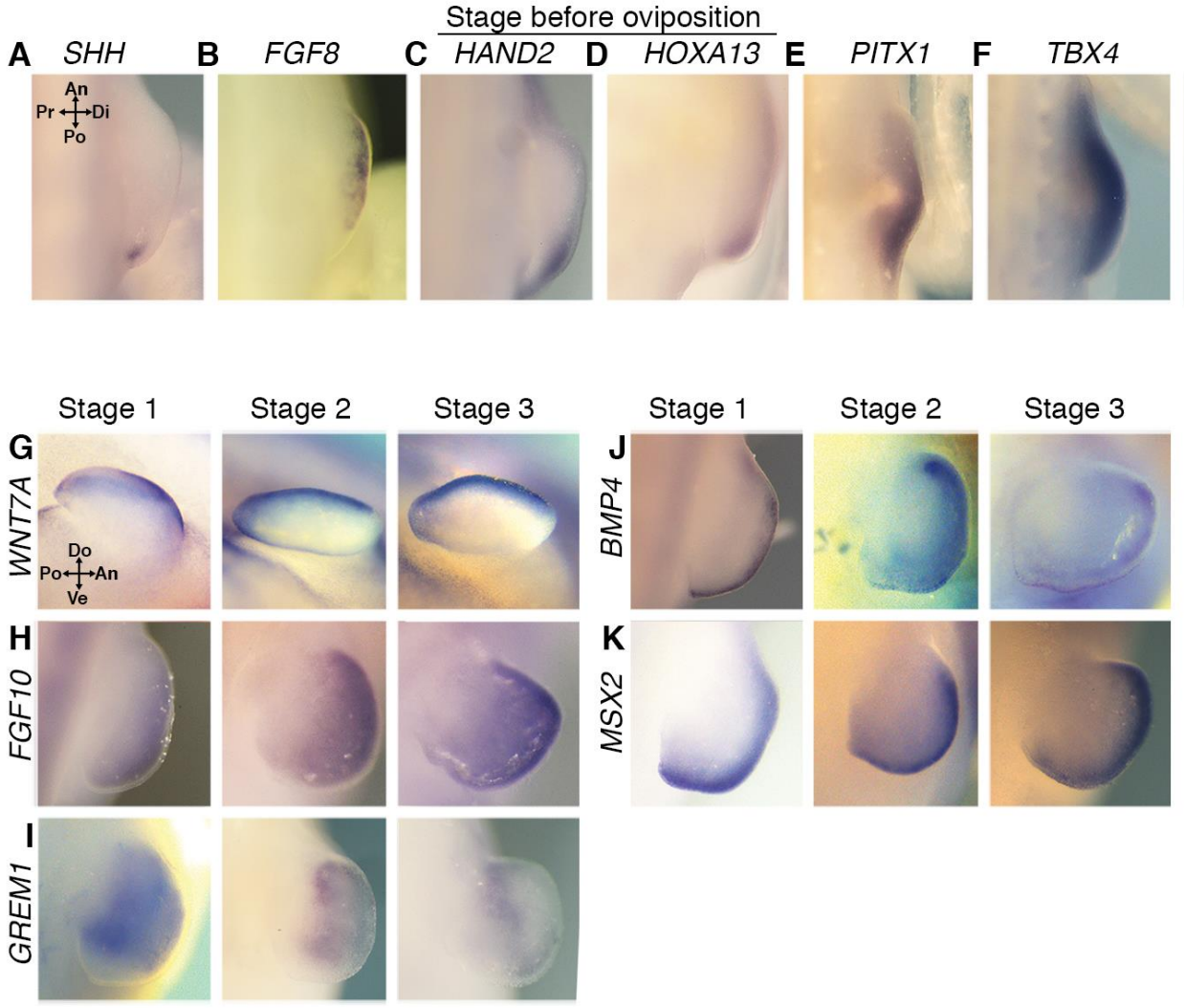

Figure S1 (Related to Figure 1 and Figure 2)

Expression of limb developmental control genes during python hindlimb development.

(A-F) Gene expression in early python hindlimb buds, at stage before oviposition. (G-K) Gene expression at post-oviposition stages. Stages are shown at top and gene names at left. Arrows show orientation of limb axes; An, anterior; Po, posterior; Do, dorsal; Ve, ventral; Pr, proximal; Di, distal.

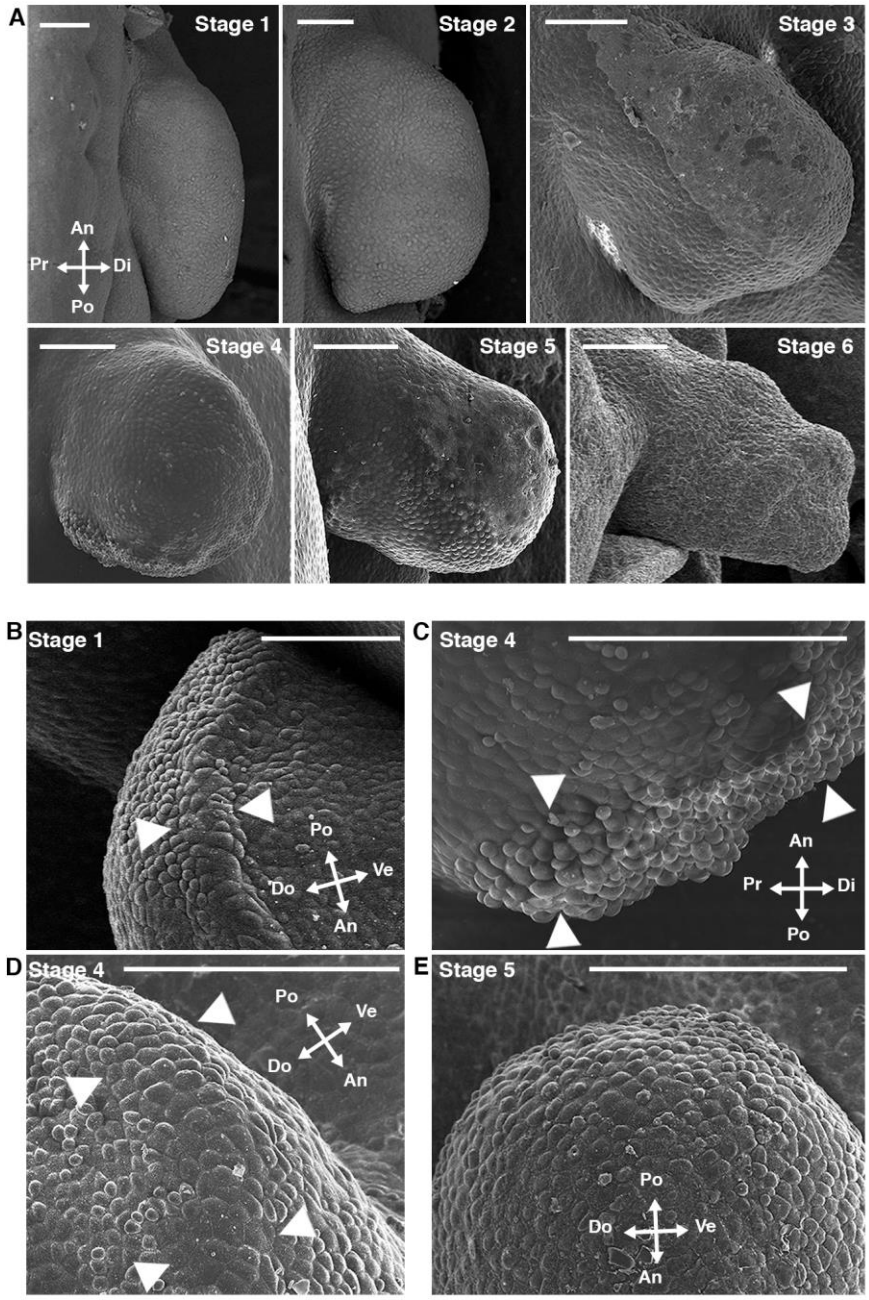

Figure S2 (Related to Figure 1)

Scanning electron microscopy (SEM) shows posterior-to-anterior degeneration of the AER in python hindlimb buds.

(A) Python hindlimb development at six embryonic stages. White arrows indicate orientation of limb axes; An, anterior; Pr, proximal; Di, distal; Po, posterior. (B) High magnification of the AER (white arrowheads) of stage 1 hindlimb bud. (C and D) Stage 4 hindlimb bud showing changes in AER structure along the anteroposterior axis. (E) Distal view of stage 5 python hindlimb bud showing that the AER has been lost along the entire anteroposterior axis. Scale bar is 100 μm.

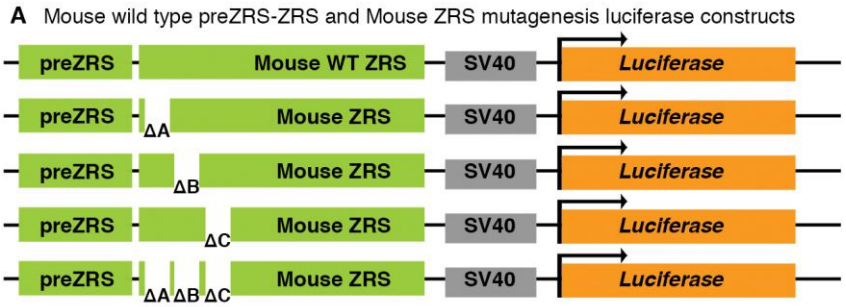

B Transactivation of preZRS-ZRS report constructs by HOXD proteins

	No *Hoxd*	*+Hoxd13*	*+Hoxd10*	*+Hoxd9*	*+Hoxd13 +d10*	*+Hoxd13 +d9*	*+Hoxd10 +d9*	*+Hoxd13 +d10+d9*
Mouse WT preZRS-ZRS	100.0	761.4	120.1	374.1	2092.9	1913.9	269.4	1055.3
Mouse preZRS-ZRS with Python ΔA	53.2 *P=5.2x10^{-10}*	617.0 *P=0.057*	84.5 *P=0.017*	133.3 *P=0.013*	768.0 *P=0.030*	863.0 *P=0.0011*	139.8 *P=0.0050*	546.6 *P=2.3x10^{-5}*
Mouse preZRS-ZRS with Python ΔB	78.8 *P=4.4x10^{-8}*	622.9 *P=0.0071*	32.6 *P=0.0019*	73.7 *P=0.0065*	308.3 *P=0.0045*	366.9 *P=3.0x10^{-4}*	94.1 *P=0.0090*	417.4 *P=3.2x10^{-5}*
Mouse preZRS-ZRS with Python ΔC	19.6 *P=3.0x10^{-6}*	197.4 *P=1.7x10^{-4}*	29.3 *P=0.0012*	20.5 *P=0.0050*	102.0 *P=0.0038*	123.9 *P=1.7x10^{-4}*	39.0 *P=0.0040*	158.9 *P=1.3x10^{-5}*
Mouse preZRS-ZRS with Python ΔABC	12.8 *P=8.7x10^{-10}*	35.6 *P=8.0x10^{-5}*	5.3 *P=0.0011*	7.9 *P=0.0041*	31.1 *P=0.0040*	24.4 *P=1.4x10^{-4}*	5.4 *P=0.0049*	22.5 *P=2.7x10^{-5}*

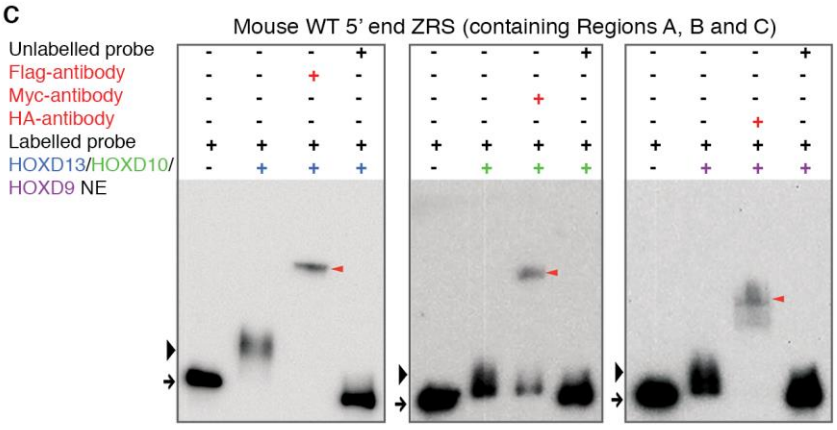

Figure S3 (Related to Figure 3)
Analysis of mutations in the python ZRS using luciferase reporters and binding assays with HOXD proteins. (A) Five constructs for luciferase reporter assays. Firefly luciferase reporter vectors contain the wild type mouse preZRS and ZRS regions, either unmodified in the control (top) or with site-directed mutations that reproduce the three python ZRS deletions, ΔA, ΔB, and ΔC, individually (middle 3) or together (bottom). ΔC also contains the RegionC microduplication found in pythons. (B) Relative transactivation values of preZRS-ZRS reporter constructs by HOXD proteins. In each cell, top: mean values; bottom: P values. Mean values are shown as percentages, normalized to the mouse wild type preZRS-ZRS without Hoxd overexpression. Two-tailed t-test, n=4 (C) Electrophoretic mobility shift assay (EMSA) using the wild type mouse 5' ZRS (~400 nt, which includes RegionA, RegionB and RegionC; see Figure S4 for complete oligonucleotide sequence) together with nuclear extracts from cells transfected with *Hoxd13-3XFlag*, *Hoxd10-3XMyc* and *Hoxd9-3XHA*. Black arrowheads indicate gel shift; red arrowheads indicate supershift.

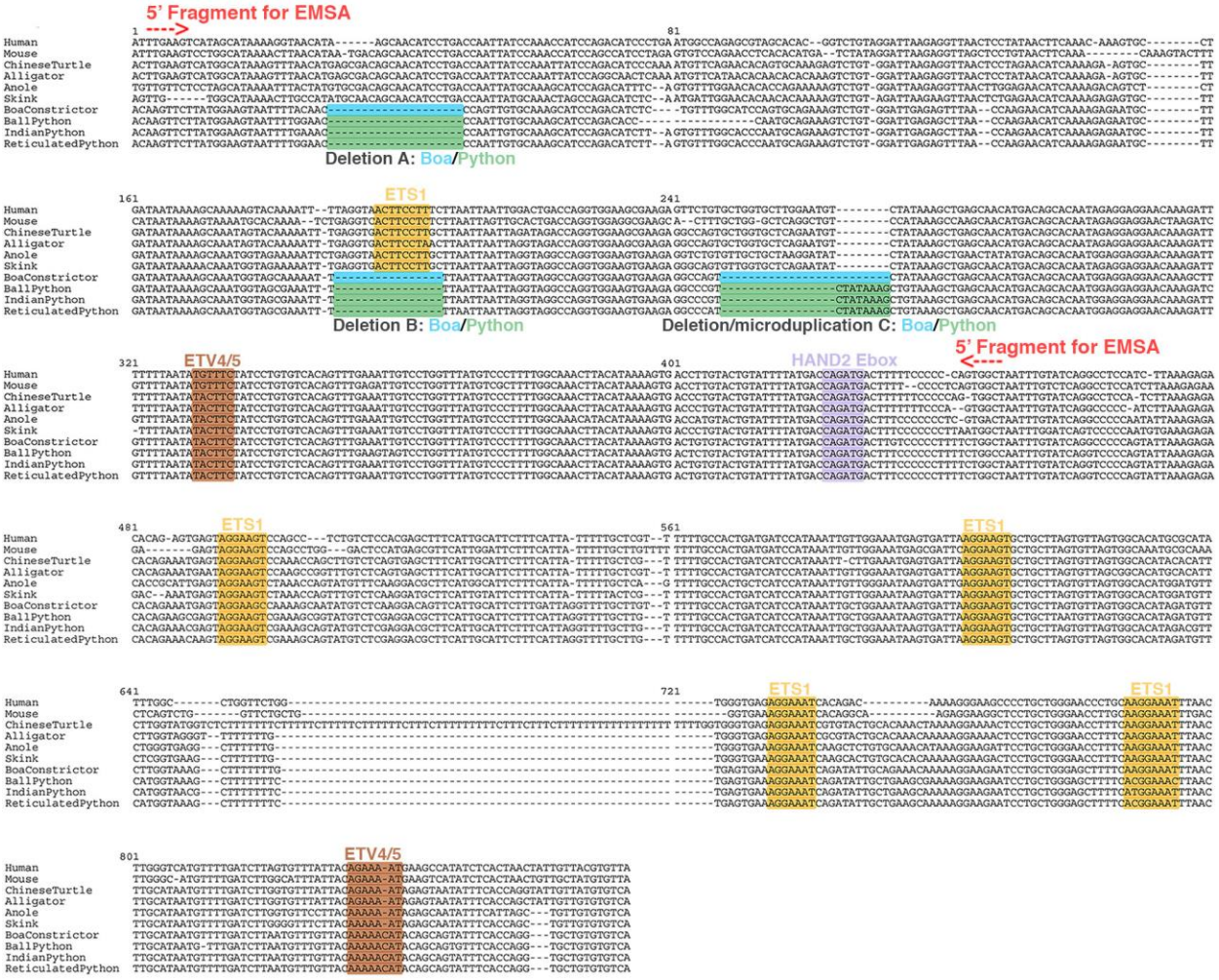

Figure S4 (Related to Figure 2 and Figure 3)

Multiple Sequence Alignment of ZRS from multiple vertebrate species, including three different python species and one boa. Species are shown at left. Deletions A, B, and C are highlighted in blue and green for python and boa (python ΔC includes microduplication). Transcription factor binding sites outside of the deletions are annotated and highlighted. Region used for EMSA experiments in Figure 3 and Figure S3 is indicated by red arrows.

Supplemental Experimental Procedures

Embryo collection and processing

Freshly laid eggs from *Python regius* were purchased from a commercial supplier or collected from our python breeding facility. Eggs at pre-oviposition stages were harvested from euthanized gravid females. Eggs from *Anolis sagrei* were collected from our breeding facility. Eggs were incubated, staged, and processed for *in situ* hybridization as previously described [S1]. Isolation of RNA and DNA for gene cloning was performed as previously described [S1]. PCR primer sequences are provided in Supplemental Experimental Procedures List 1. Whole mount *in situ* hybridization for *P. regius* and *A. sagrei* were performed as previously described [S2] and [S1]. *P. regius* embryos used for section *in situ* hybridizations were embedded in OCT, cryosectioned at 12 um, and processed as previously described [S2]. SEM imaging of python embryos was conducted as previously described [S1].

Analysis of apoptosis

Freshly dissected python and anole embryos were incubated at room temperature in 10 ml of PBS containing 50 ul of LysoTracker® Red DND-99 (L-7528, Life Technologies) for 30-60 minutes, depending on the embryonic developmental stage. Embryos were washed in PBS, fixed in 4% PFA overnight, and then washed in PBS, dehydrated in a graded methanol series, and imaged in 100% methanol.

Optical Projection Tomography (OPT)

Snake and lizard embryos were fixed in 4% paraformaldehyde in PBS. Skeletal staining for bone and cartilage was performed as described [S3] without the final glycerol steps. Specimens were cleared in 1% KOH, washed in PBS, and processed for OPT as described previously [S4, 5]. OPT scanning was performed using a Bioptonics 3001 OPT Scanner. OPT images were reconstructed using NRecon software and imported into Amira® for 3D visualization, analysis, and rendering of 3D images.

Sequence analysis of conserved non-coding DNA regulatory elements

Long global alignments of the ZRS and *Hoxd13* regulatory loci were generated and represented by curve-based visualization of sequence similarity using mVISTA software [S6]. Default parameters in the VISTA browser plot were used to calculate conserved regions and to display VISTA graphs. The ZRS sequences used for the VISTA analysis were extracted from annotated *Lmbr1* genes in NCBI or from the genome assemblies for Chinese softshell turtle (PelSin_1.0, Ensembl Genome Browser), anole lizard (AnoCar2.0, Ensembl Genome Browser), Burmese python (version 5.0.2, NCBI), king cobra (OphHan1.0, NCBI), pit viper (P.Mucros1.0, NCBI), garter snake (Thamnophis sirtalis-6.0, NCBI) and boa constrictor (assembly version 1C, Assemblathon2, http://gigadb.org). Regions of interest were isolated using standalone Blast [S7]. *Lmbr1* intron 5 was amplified from python (*Python regius*) and skink *(Mabuya sp*) genomic DNA by PCR using the following primers: Exon 5 Forward 5'TTCCAATCTTTGTTTGTTTGTATTGATGCC3'; Exon 6 Reverse 5'TGCAGCATCATTGTCTATGAGAGCTGAAGC3'.

Transgenic mice

Green anole lizard (*A. carolinensis*) and python (*P. regius* and *P. reticulatus*) pZRS-ZRS were cloned into an HSP68-LacZ reporter vector, upstream of a HSP68 minimal promoter and a LacZ reporter gene. The primers used for PCR amplification of the preZRS-ZRS region from *Python regius* were: Forward 5'ACAGCATCAAAATGGTGGGTGCTTCC3'; Reverse 5'ATTGTGAAGTAGCCCCTTGTTGCTCACC3'; and from *Anolis carolinensis*: Forward 5'AGTTTCTCCTTGCACTTAGGCT3'; Reverse 5'CTTGGTTGCTGTACATTCTCACA3'. Transgenic embryos were generated by pronuclear injections by Cyagen Biosciences Inc. or the University of Florida Animal Care Services Mouse Models Core and were collected at embryonic day 10.5 to 11.5, genotyped, and X-gal stained. Numbers of LacZ-positive/PCR-positive transgenic

mouse embryos at each stage are as follows: *Anolis* preZRS-ZRS construct: E10.5 - 1/5; E11.0 - 9/17; E11.5 - 18/26; *Python* preZRS-ZRS construct: E10.5 - 0/31; E11.0 - 0/14; E11.5 - 3/24.

Vector construction

Expression vectors for Hoxd13, Hoxd10 and Hoxd9 proteins were produced using full-length cDNAs synthetized from total RNA extracted from embryonic day 11.5 mouse lumbar to tail regions (See DNA primer sequences in Supplemental Experimental Procedures List 2). PCR amplification was performed using the following proofreading DNA polymerase mixes: Advantage 2 (639201, Clontech) for *Hoxd10* and *Hoxd9* and Advantage® GC 2 (639114, Clontech) for *Hoxd13*. Full-length amplicons were then cloned into a pCMV-pcDNA^{TM}3.3-TOPO expression vector (K8300-01, Invitrogen). Epitope-tagged fusion proteins were made by adding the corresponding amino acid sequences to the 5' end of the reverse primers and PCR was used to generate epitope-tagged full-length cDNAs.

Firefly luciferase reporter vectors for preZRS-ZRS elements were created by PCR amplification from genomic DNA extracted from mouse, anole, and python tissue (Primers used for PCR amplification of the preZRS-ZRS region from *Mus musculus*: Forward 5' TTACAGGAAAGCTACAAAGGGTGCTAGCA3'; Reverse 5'CGTCACAGAAGAACAGCGCTACCGTGGCT3'). These elements were cloned into a pGL4.13 firefly luciferase reporter vector, upstream of an SV40 promoter, to control firefly luciferase transcription (E6681, Promega).

Mouse ZRS site-directed mutagenesis

Firefly luciferase reporter vectors containing the mouse preZRS-ZRS with the three python deletions were created by splitting the mouse preZRS-ZRS into three consecutive DNA fragments (A, B, and C) that were assembled as a single insert (5'-ABC-3') into the pGL4.13 firefly luciferase reporter vector. Only the middle fragment (B) carried the three python deletions. Fragments A and C were composed of the 5' and 3' wild-type sequences, respectively. The wild-type fragments A and C were PCR amplified from mouse genomic DNA. Fragment B was chemically synthetized (IDT, Integrated DNA Technologies) as to complementary oligonucleotides of ~200 bp, and hybridized in an oligonucleotide annealing reaction using equimolar concentrations of each complementary oligonucleotide in a Tris/EDTA buffer (10 mM Tris, pH 7.4; 1mM EDTA; See DNA primer and oligonucleotides sequences in Supplemental Experimental Procedures List 3). To assemble the three fragments in the correct order and into the firefly luciferase reporter vector, we used InFusion cloning (Clonetech). Infusion reactions were used to transform competent DHα *E. coli* cells for bacterial vector cloning. The correct assembly of the mutated mouse preZRS-ZRS was confirmed by Sanger sequencing from plasmid DNA isolated from transformed bacterial cells.

Luciferase assays

Firefly luciferase reporter activity of the PreZRS-ZRS vectors was studied in mouse NHI3T3 fibroblast cells (CRL-1658, ATCC) grown at 37 °C and 5% CO_2 in Dulbecco's Modified Eagle's Medium (ATCC #30-2002) supplemented with 10% bovine serum (ATCC #30-2030), antibiotics and antimycotic (1,000 units of penicillin, 1 mg/ml streptomycin and 2.5µg/ml Amphotericin B; Sigma-Aldrich# A5955). Cells were transfected with Hoxd expression vectors, firefly luciferase and renilla luciferease plasmids with lipofectamine 3000 (Invitrogen# L3000008) following manufacturer instructions. Cells were grown to approximately 70 % confluence in 48 well plates after transfection. The Dual-Luciferase® Reporter (DLR™) assay system (E1960, Promega) was used to produce nuclear lysates and luminescence reactions from firefly and renilla luciferases, following manufacturer instructions. Nuclear lysates were measured in 96-well plates using a BMG Fluorstar OPTIMA microplate reader.

Electrophoretic mobility shift assay

Hoxd proteins were overexpressed in NIH3T3 cells by transfection of the corresponding expression vector (*Hoxd13*, *Hoxd10* and *Hoxd9*), and then cells were grown for 48 hours in T-25 flasks. Nuclear lysates were isolated using the NE-PER Nuclear and Cytoplasmic Extraction Kit (78833, ThermoFisher) following manufacturer instructions. To assay Hoxd binding to the three regions of the wild type mouse ZRS regions that are deleted in python deletions, we first tested a ~400 nt fragment amplified from the 5'end of the wild type mouse ZRS, as described [S8] (See Figure S4 and Supplemental Experimental Procedures List 4). To narrow down the binding to individual python deletions within the 5'end of the wild type mouse ZRS, three 40 nt probes were designed to overlap python deletion regions A, B, and C (See DNA primers and oligonucleotides sequences in Supplemental Experimental Procedures List 4). Biotin labeling of DNA probes was performed using the Biotin 3' End DNA Labeling Kit (89818, ThermoFisher) following manufacturer instructions. Protein-DNA binding reactions and electrophoretic shift detection on nylon membranes (ThermoFisher # 77016) were performed using the LightShift™ Chemiluminescent EMSA Kit (ThermoFisher # 20148) following manufacturer instructions. For super-shift experiments with epitope tagged proteins, we used anti-FLAG (ab18230, Abcam), anti-Myc (ab18185, Abcam), and anti-HA (ab1424, Abcam) antibodies. Gel electrophoresis was performed using 5% polyacrylamide precast gels (Biorad# 4565015) in TBE buffer, and gel transfer to a nylon membrane was performed using the Trans-Blot® Turbo™ Transfer System (Biorad).

SUPPLEMENTAL REFERENCES

S1. Leal, F., and Cohn, M.J. (2015). Development of hemipenes in the ball python snake Python regius. Sex Dev *9*, 6-20.

S2. Nieto, M.A., Patel, K., and Wilkinson, D.G. (1996). In situ hybridization analysis of chick embryos in whole mount and tissue sections. Methods in cell biology *51*, 219-235.

S3. Wassersug, R.J. (1976). A procedure for differential staining of cartilage and bone in whole formalin-fixed vertebrates. Stain Technol *51*, 131-134.

S4. Quintana, L., and Sharpe, J. (2011). Preparation of mouse embryos for optical projection tomography imaging. Cold Spring Harbor protocols *2011*, 664-669.

S5. Quintana, L., and Sharpe, J. (2011). Optical projection tomography of vertebrate embryo development. Cold Spring Harbor protocols *2011*, 586-594.

S6. Frazer, K.A., Pachter, L., Poliakov, A., Rubin, E.M., and Dubchak, I. (2004). VISTA: computational tools for comparative genomics. Nucleic Acids Res *32*, W273-279.

S7. Altschul, S.F., Gish, W., Miller, W., Myers, E.W., and Lipman, D.J. (1990). Basic local alignment search tool. J Mol Biol *215*, 403-410.

S8. Capellini, T.D., Di Giacomo, G., Salsi, V., Brendolan, A., Ferretti, E., Srivastava, D., Zappavigna, V., and Selleri, L. (2006). Pbx1/Pbx2 requirement for distal limb patterning is mediated by the hierarchical control of Hox gene spatial distribution and Shh expression. Development *133*, 2263-2273.

Supplemental Experimental Procedures List 1. Primers used to PCR clone *in situ* hybridizations probes for *Python regius* and *Anolis sagrei* embryos.

	Python regius	*Anolis sagrei*
SHH Forward	ATACGAGGGCAAGATCAGCCGGAAC	GACCCCTCTGGCCTACAAGCAGTTT
SHH Reverse	GCTGCTTGTAACAGTGTCTGACCCC	CAAAGATGGGCTGGGGTTGGGAATG
PTCH1 Forward	ATGTTCGCACCTGTGTTGGATGGAG	CACCTGTGTTGGATGGAGCTGTGTC
PTCH1 Reverse	GTTGGCAACATGGTGGCACAGAAGA	TTGGCAACATGGTGGCACAGAAGAG
GLI1 Forward	CAGCCACTGCTGCTCTTGCACCCTG	CAGCCACTGCTGCTCTTGCACCCTG
GLI1 Reverse	AGGGTATTAAGGAACTGGTTCTCCCCTGC	AGGGTATTAAGGAACTGGTTCTCCCCTGC
FGF8 Forward	TACACAGCATGTGAGGGAGCAGAGC	TACACAGCATGTGAGGGAGCAGAGC
FGF8 Reverse	GCTTTGGGCTGGAGTTTCGAGTCCT	GCTTTGGGCTGGAGTTTCGAGTCCT
GLI3 Forward	CAGTGTGATGGCTTGCCTGGACTTC	CAAATAGCAGCTGCAGTGTCGGAGG
GLI3 Reverse	CAGCTGCTGCTGGACAACCATGTTA	TTCTGTGGTAGCAGCCTCCATAGCC
HAND2 Forward	GCGCAGGACTCAGAGCATCA	GCGCAGGACTCAGAGCATCA
HAND2 Reverse	CGGGTGACACTGACCAGCTC	CGGGTGACACTGACCAGCTC
HOXD13 Forward	GAGAAGTACATGGACGTGGCCG	GAGAAGTACATGGACGTGGCCG
HOXD13 Reverse	TGGAGCAGTACACCTGCCCGTT	TGGAGCAGTACACCTGCCCGTT
HOXA13 Forward	GCGGCTGCAGGCACCAA	GAAGCGGGCTTCCACGC
HOXA13 Reverse	GCCGCCACCGACGTCTC	ATGTACTTGTCGGCGAAGGAG
SOX9 Forward	CACACACTCACCACCCTGAGTAGCG	ACTCACCACCCTGAGTAGCGAACCA
SOX9 Reverse	GTGAGCTGTGTATAGACTGGCTGTTCCC	TCTGGTGAGCTGTGTATAGACTGGCTGT
PITX1 Forward	CAACCAGCAGATGGACCTTTG	
PITX1 Reverse	CTGTTGTACTGGCAGGCGTTTAG	
TBX4 Forward	CAACAGCCCTTTCTCGGTCTAC	
TBX4 Reverse	ACCCGTCAGTCCAGTTGTCC	
WNT7a Forward	GTGTCAGGATCATGCACTACTAA	
WNT7a Reverse	ACAGGTGTAGACTTCTGTTCGTT	
FGF10 Forward	ATATTGGAAATAACATCTGTGGAAATTGGAG	
FGF10 Reverse	CGACTACCATGGGAAGAAATGAGCAGT	
GREM1 Forward	GGCTTGCACAGTTTCTGCTGTTGGTG	
GREM1 Reverse	GATATACAGCGGCATTCTTTAACTCGTGTG	
BMP4 Forward	CCGCGCAAGAGCAAGAAGAA	
BMP4 Reverse	TCCCTCTACGACCATTTCCTGG	
MSX2 Forward	GAGTCCCACAGCCTGTACACTAAG	
MSX2 Reverse	CTACAGGTGGGATAGGAAGCACAG	

Supplemental Experimental Procedures List 2. Primers used for amplification of full-length coding sequences of mouse *Hoxd13* (NM_008275), *Hoxd10* (NM_013554) and *Hoxd9* (NM_013555) genes to construct expression vectors.

Hoxd13 **Forward**	GCCACGATGAGCCGCTCGGGGACTTGGGAC
Hoxd13 **Reverse3xFlag**	TCCAAGCTCAAAGACACTGTCTCCGACTACAAAGACGATGACGACAAGGATTATAAGGATGATGATGATAAAGACTACAAAGACGATGACGACAAGTAG
Hoxd10 **Forward**	CCCAAAATGTCCTTTCCCAACAGCTCTCCT
Hoxd10 **Reverse3xc-Myc**	CTGACCGCCAACCTCACCTTTTCTGAACAAAAACTCATCTCAGAAGAGGATCTGGAGCAGAAGTTGATAAGTGAGGAAGACTTAGAACAAAAACTCATCTCAGAAGAGGATCTGTAG
Hoxd9 **Forward**	CTCACCATGTCGTCCAGTGGCACCCTCAGC
Hoxd9 **Reverse3xHA**	AAGGAGAAGTGCCCTAAAGGAGACTACCCATACGATGTTCCAGATTACGCTTATCCCTATGACGTGCCCGACTATGCGTACCCATACGATGTTCCAGATTACGCTTAG

Supplemental Experimental Procedures List 3. Primers used for mouse ZRS site-directed mutagenesis in preZRS-ZRS luciferase reporter experiments.

Mouse WT 5'end preZRS Forward	TGGCCGGTACCTGAGTTACAGGAAAGCTACAAAGGGTGCTAGCA
Mouse WT 3'end ZRS Reverse	CTGCGCAGATCTGATCGTCACAGAAGAACAGCGCTACCGTGGCT
Mouse ZRS Region A with Python ΔA Reverse	GGTTTGGATAATTGGATGTTAAGTTTTATGCCAGGACTT
Mouse ZRS Region A with Python ΔA Forward	CCAATTATCCAAACCATCCAGCCATCCT
Mouse ZRS Region B with Python ΔB Reverse	AGTGCAACTAATTAAAGATTTTGTGCATTTTACTTTTAT
Mouse ZRS Region B with Python ΔB Forward	TTAATTAGTTGCACTGACCAGGTGGAGG
Mouse ZRS Region C with Python ΔC Reverse	TGTTGCTTGGCTTTACAGCTTTATGGAAAGTGCTTCGCCTCCACCTGGTC
Mouse Region C with Python ΔC Forward	TAAAGCCAAGCAACATGACAGCACAATA
Mouse ZRS Region ABC with Python ΔABC, Sense oligonucleotide	TCCAATTATCCAAACCATCCAGCCATCCTAGAGTGTCCAGAACCTCACACAT GATCTATAGGATTAAGAGGTTAGCTCCTGTAACTTCAAACAAAGTACTTTCA TAATAAAAGTAAAATGCACAAAATCTTTAATTAGTTGCACTGACCAGGTGG AGGCGAAGCACTTTCCATAAAGCTATAAAGCCAAGCAACA
Mouse ZRS Region ABC with Python ΔABC, Antisense oligonucleotide	TGTTGCTTGGCTTTATAGCTTTATGGAAAGTGCTTCGCCTCCACCTGGTCAGT GCAACTAATTAAAGATTTTGTGCATTTTACTTTTATTATGAAAGTACTTTGTT TGAAGTTACAGGAGCTAACCTCTTAATCCTATAGATCATGTGTGAGGTTCTG GACACTCTAGGATGGCTGGATGGTTTGGATAATTGGA

Supplemental Experimental Procedures List 4. Probes used in EMSA experiments with wild type mouse ZRS oligonucleotides containing regions A, B, C, and ABC. 3' end biotinylation of sense (S) and antisense (AS) oligonucleotides was performed before oligo hybridization. Primers were used to amplify the wild type mouse 5' ZRS fragment containing the regions corresponding to those deleted in python A, B, and C mutations.

Mouse WT ZRS RegionA Sense	GACAGCAACATCCTGACCAATTATCCAAACCATCCAGCCA
Mouse WT ZRS RegionA Antisense	TGGCTGGATGGTTTGGATAATTGGTCAGGATGTTGCTGTC
Mouse WT ZRS RegionB Sense	CTGAGGTCACTTCCTCTCTTAATTAGTTGCACTGACCAGG
Mouse WT ZRS RegionB Antisense	CCTGGTCAGTGCAACTAATTAAGAGAGGAAGTGACCTCAG
Mouse WT ZRS RegionC Sense	GCACTTTGCTGGGCTCAGGCTGTCCATAAAGCCAAGCAAC
Mouse ZRS RegionC Antisense	GTTGCTTGGCTTTATGGACAGCCTGAGCCCAGCAAAGTGC
Mouse WT 5'end ZRS Regions ABC Forward	CTTTGATTTGAAGTCCTGGC
Mouse WT 5'end ZRS Regions ABC Reverse	ACTGAGGGGAAAAGTCATC